Research Square

Preprints are preliminary reports that have not undergone peer review.
They should not be considered conclusive, used to inform clinical practice,
or referenced by the media as validated information.

Drivers of Decadal Sea-level Variability in the Southwestern Tropical Indian Ocean

SAJIDH CK

sajidh.c.k@gmail.com

Indian Institute of Technology Madras https://orcid.org/0009-0002-1589-0635

Nidheesh Gangadharan

ESSO- Indian National Centre for Ocean Information Services

Abhisek Chatterjee

ESSO- Indian National Centre for Ocean Information Services

Research Article

Keywords: Decadal sea-level variability, Indian Ocean, ENSO-Modoki, Atmospheric Teleconnections

Posted Date: June 9th, 2026

DOI: https://doi.org/10.21203/rs.3.rs-9624475/v1

License: This work is licensed under a Creative Commons Attribution 4.0 International License.
Read Full License

Drivers of Decadal Sea-level Variability in the Southwestern Tropical Indian Ocean

C. K. Sajidh[1,2,*], A. G. Nidheesh[2], C. Abhisek[2]

[1] Indian Institute of Technology, Madras. Chennai
[2]Indian National Centre for Ocean Information Services, Hyderabad, India

Corresponding author: sajidh.c.k@gmail.com

Abstract

In the tropical Indian Ocean, the Southwest Tropical Indian Ocean (SWIO; 5°S–20°S) exhibits the highest sea-level variance at decadal time scales. Previous studies found that wind stress curl (WSC) variability over the central and Southeast Indian Ocean (SEIO) plays a key role in driving sea-level anomalies (SLA) in the SWIO, with some studies also indicating a contribution from Rossby waves radiating from the eastern boundary of the basin. While the influence of Pacific and Indian Ocean wind variations on SWIO decadal sea-level variability has been recognized, their relative roles remain unclear. This study demonstrates that remotely forced decadal WSC anomalies over the SEIO are largely associated with central Pacific El Niño (ENSO Modoki), with canonical ENSO playing a secondary role. After removing the Pacific contribution, the residual variability is associated with a meridional tripolar sea-level pressure pattern and corresponding wind anomalies in the Indian Ocean. We derive an index based on sea-level pressure, called the Indian Ocean Decadal Index (IDI), that effectively captures the intrinsic decadal sea-level variability in the tropical Indian Ocean. A linear regression model incorporating Pacific climate forcing (ENSO and ENSO Modoki) and IDI explains over 80% of the observed decadal sea-level variance in the SWIO, providing a valuable framework for Indian Ocean decadal prediction

Keywords: Decadal sea-level variability, Indian Ocean, ENSO-Modoki, Atmospheric Teleconnections.

1. Introduction

The southwest Tropical Indian Ocean (SWIO; 5°S-15°S) is characterized by a persistent open-ocean upwelling and a climatological sea-level low, often referred to as the Seychelles-Chagos thermocline ridge (e.g., Hermes & Reason, 2009). The annual-mean thermocline in the SWIO is remarkably shallow (~80 m) in response to the prevailing southeasterlies (to the south of about 8°S) and equatorial westerlies in the tropical Indian Ocean (IO), with no clear signature on sea surface temperature (SST; e.g., McCreary et al., 1993; Praveen Kumar et al., 2014; Tozuka et al., 2010). It is found that the upwelling in the SWIO is just not a response to the divergence driven by local wind-stress curl (WSC), but also modulated by remotely forced oceanic Rossby waves propagating from the eastern IO (e.g., Masumoto & Meyers, 1998; Mukhopadhyay et al., 2022). At interannual time scales, the anomalous upwelling in the SWIO affects sea surface temperature (SST) as well, exhibiting strong air-sea coupling and plays a key role in modulating the climate over the IO rim (Rao and Behera, 2005; Vialard et al., 2009; Chowdary et al., 2009; Xie et al., 2002, 2009).

The interannual sea-level variability in the SWIO is primarily driven by the anomalous WSC in the tropical SIO linked to the two leading climate modes: the El Niño Southern Oscillation (ENSO) and the Indian Ocean Dipole (IOD; McPhaden et al., 1999; Saji et al., 1999; Webster et al., 1999; Masumoto & Meyers, 1998; Schott et al., 2009; Tozuka et al., 2010; Nidheesh et al., 2013). The interannual WSC anomalies in the SIO drive anomalous Ekman pumping that propagates westward as Rossby waves, altering the mean thermocline and sea level in the SWIO (Masumoto & Meyers, 1998; Tozuka et al., 2010). Though both IOD and ENSO trigger anomalous winds in the equatorial and south IO: the IOD events drive sea-level anomalies (SLA) north of 10°S, while the ENSO-driven wind and SLA are largely confined to south of 10°S (Rao & Behera, 2005; Yu et al., 2005). It is found that the equatorial easterly anomalies associated with a positive IOD and El Niño drive SLA in the eastern equatorial IO (EEIO) and along the rim of the Bay of Bengal (BoB) through Kelvin waves (Rao et al., 2009; Aparna et al., 2012; Nidheesh et al., 2013). A large number of studies have shown that the SLA in the western tropical Pacific during the ENSO cycle propagates into the southeast IO via the coastal waveguide (Clarke, 1991; Clarke & Liu, 1993; Meyers, 1996; Masumoto & Meyers, 1998; Potemra, 2001, 2002; Feng et al., 2003; Wijffels & Meyers, 2004; Cai et al., 2005; Nidheesh et al., 2013) and thenradiate westward as Rossby waves into the interior SIO basin, impacting sea level and upper-ocean heat content of SIO (Masumoto & Meyers, 1998; Wijffels & Meyers, 2004). Thus, ENSO influences the SLA in the SWIO through both atmospheric and oceanic teleconnections.

Several studies have examined decadal heat content and sea-level variability in the SIO, showing broad agreement that local wind variations play a key role in driving decadal SLA in the SWIO, while offering differing interpretations of how Pacific variability influences SWIO SLA through atmospheric and oceanic teleconnections (e.g., Han et al., 2006; Alory et al., 2007; Lee & McPhaden, 2008; Zhuang et al., 2013; Han et al., 2010; Trenary & Han, 2012; Nidheesh et al., 2013; Li & Han, 2015; Schwarzkopf & Böning, 2011; Deepa et al., 2018; Ummehofer et al., 2017; Jin et al., 2018; Jayasankar et al., 2019; Nidheesh et al., 2022). For example, few studies have indicated the significant role of oceanic bridge (ITF and coastal wave guide connecting western Pacific and the west Australian coast) in linking the Pacific variability to SLA in the SWIO via Rossby wave dynamics (e.g., Alory et al. 2007; Schwarzkoph & Boning, 2011; Ummehofer et al. 2017), while other suggest the locally and remotely driven wind stress curl in the SIO as the main driver of SLA and heat content in the SWIO with minimal

or no contribution from Pacific oceanic bridge (e.g., Han et al. 2006; Nidheesh et al., 2013; Jin et al. 2018; Zhuang et al. 2013; Deepa et al., 2018). The multi-decadal sea-level fall in the SWIO during the last decades of the twentieth century (e.g., Han et al. 2010) was linked to changes in the Indian Ocean atmospheric circulation, partly attributed to anthropogenic warming in the Indo-Pacific region (Alory et al., 2007; Barnett et al., 2005; Han et al., 2006, 2010; Pierce et al., 2006; Trenary & Han, 2008).

In this study, we investigate the drivers of decadal sea-level variations in the SWIO using outputs from an ensemble reanalysis over the 1960 – 2023 period. Our major finding is that sea surface warming in the central Pacific plays a key role in driving SWIO sea level through anomalous zonal circulation in the Indo-Pacific. Our results also provide insights into the intrinsic sea-level variability in the IO. A regression model combining the Pacific and IO forcing can explains nearly 80% of the SWIO decadal sea-level variations. The paper is structured in this format. Section 2 provides a detailed description of the data and methodology adopted in this study. We present the main findings in Section 3. Section 4 provides a discussion, and Section 5 presents a conclusion.

2. Data and Methods

2.1. Data

We used sea surface height (SSH) from three ocean reanalysis products: the ORA-S5 (Zuo et al., 2019; for the period 1960 – 2023), GECCO3 (Köhl, 2020; 1960–2018), and SODA 2.2.4 (Carton et al., 2018; 1960–2010), all employing volume conservation in their base ocean model. We removed global-mean sea level (GMSL) from each reanalysis's SSH to obtain the dynamic sea level (DSL). Hereafter, sea-level anomaly (SLA) represents dynamic sea level (DSL).. Even though each reanalysis product covers a different period, we constructed an ensemble mean of these three products so that our ensemble-mean DSL covers the full period (1960 – 2023). Although ocean reanalysis products are strongly constrained by available observations, the relatively sparse observational coverage in the Indian Ocean—particularly at subsurface levels—introduces greater uncertainty. Considering multiple products helps account for uncertainties arising from model physics, forcing fields, and data assimilation.. Surface wind fields and sea-level pressure (SLP) are obtained from the ERA5 reanalysis (1940 - present, Hersbach et al., 2020).

Sea-level anomalies (SLA) from satellite altimetry, obtained from the Copernicus Marine Environment Monitoring Service (CMEMS), which is based on a merged product from multiple satellite missions, and sea level data from three selected tide-gauge records obtained from the Permanent Service for Mean Sea Level (PSMSL, Holgate et al. 2013; PSMSL, 2025) are used to validate the sea level from the reanalysis products. The selected tide-gauge stations, as shown in Fig. 1a, are Zanzibar (39°E, 6°S), Langkawi (99°E, 6.5°N), and Fremantle (115°E, 32°S). SLA from ensemble reanalysis is averaged over a 1-degree circle around each selected gauge record for comparison (Fig. S1). Similarly, box-averaged SLA (boxes shown in Fig. 1a) from both reanalysis and altimeter data are compared. In addition, sea surface temperature (SST) from the Hadley Centre Sea Ice and Sea Surface Temperature dataset (HadISST v1.1), available since 1900, is used to calculate the climate indices discussed in the paper.

2.2 Methods

We removed the monthly climatology and then applied a Butterworth lowpass filter with a 7-year cutoff to define decadal variability for all variables discussed in this paper (the frequency response diagram is shown in Fig S2). We also removed a linear trend from all low-pass-filtered variables to eliminate long-term changes. Similarly, we derived climate indices representing the major natural climate modes in the Indian and Pacific Oceans using Empirical Orthogonal Function (EOF) analysis of decadal SST anomalies for the 1960-2023 period. For Pacific SST variability, the EOFs are computed over 120°E-280°E and 20°S-20°N, and the normalized (divided by standard deviation) first and second Principal Components (PC1 and PC2) are taken as the EOF-based ENSO Index (EEI) and the EOF-based ENSO Modoki Index (EMI), respectively (Fig. S3). Similarly, we computed the EOF-based Dipole Mode Index (EDMI) over 10°S–20°N, 35°E–110°E. The EDMI was derived from SST fields after removing the influence of EEI and EMI using a combined linear regression model. The cross-correlation of these indices is given in Table S1.

Combined Climate Forcing

Sea level variability was modeled using a multiple linear regression framework, with standardized climate indices as independent predictors. Let $x_i(t)$ $(i = 1,2,..n)$ denote the standardized time series of the selected climate indices (e.g., EEI, EMI, and IDI, where IDI stands for Indian Ocean Decadal Index), each normalized to zero mean and unit variance over the analysis period and constructed to be mutually orthogonal. At each grid point, sea level anomalies $SL(t)$ were expressed as a linear combination of these indices:

$$SL(t) = \sum_{i=1}^{n} a_i \; x_i(t) + \varepsilon(t),$$

where a_i are the regression coefficients and $\varepsilon(t)$ represents the residual variability. Because the indices are orthogonal, each regression coefficient quantifies the independent linear contribution of the corresponding climate mode to sea level variability. The modeled sea-level time series at each grid point is therefore obtained as the linear superposition of the individual mode responses.

To quantify the "spatial fingerprint" of combined climate forcing (i.e., spatial map of regression coefficients that effectively shows the sea-level response to multiple climate modes such as ENSO and ENSO Modoki), we considered a projection-based method by constructing a combined climate index, ($I_{\text{combined}}(t)$), defined as a weighted sum of the standardized climate indices:

$$I_{\text{combined}}(t) = \sum_{i=1}^{n} w_i \; x_i(t),$$

where the weights (w) reflect the relative strength of the regression coefficients (between the respective index and sea level) and are normalized, as:

$$w_i = \frac{| \, a_i \, |}{\sqrt{\sum_{i=1}^{n} a_i^2}}.$$

The resulting combined index was subsequently standardized to a mean of 0 and a variance of 1. This standardized $I_{\text{combined}}(t)$ is then used as a single predictor in linear regressions to diagnose spatial patterns of sea-level response (e.g., Fig. 3d), along with associated responses in other dynamical fields (e.g., wind-stress curl).

This formulation fixes the relative strength (through weighted regression coefficient) while preserving each climate mode's signed temporal evolution by multiplying by the original indices. Consequently, constructive and destructive interactions among modes are retained in time, so that the combined index reflects their (climate modes) dynamically relevant relative strength. A simple arithmetic sum of indices would implicitly assume equal sea-level sensitivity to all climate modes and would not account for the regression-derived amplitude differences. This projection-based construction of the climate index (I), therefore, provides a dynamically consistent measure of combined climate forcing, suitable for diagnosing spatial patterns of sea-level response.

Statistical significance

To assess the statistical significance of our correlation and regression coefficients, the effective sample size (ESS) of the decadal time series is estimated as:

$$\text{ESS} = \text{N} / 2\text{T}$$

where N is the total length of the data (total months), and T is the time scale for which the autocorrelation of the time series falls to 1/e (~0.37; Leith, 1973). We found that the decadal sea-level time series in the SWIO typically has an ESS of ~ 11. For each pair of variables, the decorrelation timescale is computed separately from their respective autocorrelation functions. This yields individual effective sample sizes, ESS_a and ESS_b which are then combined to estimate the effective degrees of freedom as

$$DOF = \sqrt{ESS_a \times ESS_b} - 2$$

This formulation accounts for the autocorrelation present in both time series and provides a conservative estimate of the independent degrees of freedom used in the significance testing. The corresponding critical correlation values are then obtained from the Student's t-distribution using the estimated degrees of freedom. These threshold values are compared against the computed correlation coefficients to assess their statistical significance. A significance level of 90% is adopted in this study, and only correlations exceeding this threshold are considered statistically significant. The resulting significance levels are reported for the cross-correlations in Tables S1 and S2. Statistical significance is not explicitly shown on spatial maps.

3. Results

3.1. Observed decadal sea-level variability in the SWIO

We assessed the robustness of decadal sea-level variability in reanalysis by comparing SLA from the ensemble reanalysis with tide-gauge and satellite sea-level variations, as shown in Fig. S1. The reanalysis SLA, averaged in the vicinity of the tide-gauge records at Langkawi (EEIO) and Fremantle (WAC), shows good agreement with the respective tide-gauge records ($r > 0.8$), providing confidence in using reanalysis before 1993. The Zanzibar tide-gauge record is not ideal for comparing SWIO sea-level variations; however, we do not have a long record

in the region, and Zanzibar has been used by earlier studies for the same reason (Han et al., 2010). Nevertheless, it is worth noting that the multi-decadal fall in SWIO sea level during 1960 – 1990 (e.g., Han et al., 2010; Nidheesh et al., 2013) and the subsequent reversal are evident in both tide-gauge and reanalysis data (Fig. S1b). The correlation coefficient between ensemble reanalysis and satellite SLA exceeds 0.9 in all three key regions of variability (indicated by rectangles in Fig. 1a), which is not surprising, as reanalysis products (except SODA) use satellite SLA during the assimilation phase.

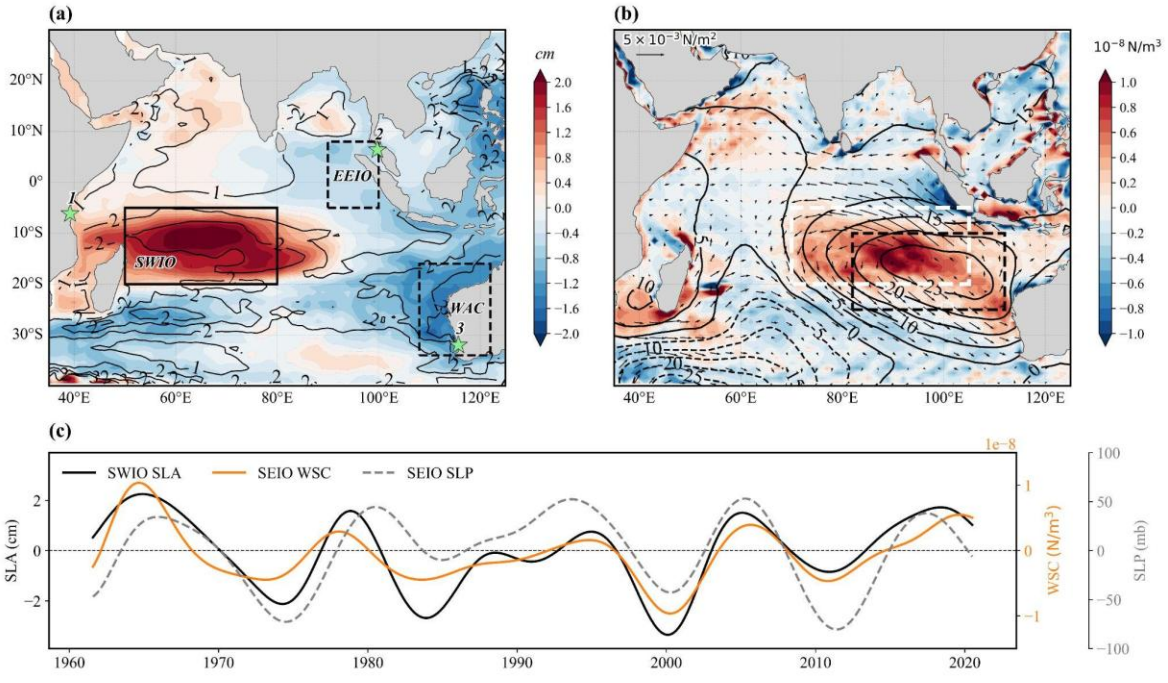


Figure 1*: (a) Regression of decadal SLA (shading) in the Indian Ocean onto the normalized (by dividing standard deviation) region-averaged SLA over the Southwest Tropical Indian Ocean (SWIO; black box), with the standard deviation of decadal SLA overlaid (contours, unit is cm). The geographic locations of selected tide-gauge stations are indicated by green stars. The dashed black boxes represent the Eastern Equatorial Indian Ocean (EEIO) and the West Australian Coast (WAC), where SLA from ensemble reanalysis and satellite altimetry are averaged for comparison. Time series of SLA from selected tide-gauge records, satellite altimetry, and ensemble reanalysis are provided in Fig. S1. (b) Regression of WSC (shading), SLP (contours; unit is in mb), and surface wind stress (vector) onto (normalised) SLA averaged in the SWIO. The key regions with the largest regression coefficients for WSC and SLP in the Southeast Tropical Indian Ocean (SEIO) are highlighted in dashed white and black rectangles, respectively. (c) Time series of regionally averaged decadal SLA in the SWIO (black box in panel a), WSC (white box in panel b), and SLP (black box in panel b).*

In the tropical IO, the amplitude of decadal sea-level variability (ranging ~ 1-3 cm standard deviation) is largest in the SWIO (Fig. 1a). The decadal sea-level variations in the SWIO are, though modestly, correlated to the eastern equatorial IO (EEIO) and off the west coast of Australia (WAC), as shown in Fig. 1a. Though interannual sea-level variability in the SWIO and EEIO is highly anti-correlated owing to the IOD dynamics (e.g., Saji et al. 1999), the SWIO-EEIO co-variability has been shown to be weak at decadal time scales (e.g., Nidheesh et al. 2013), consistent with Fig. 1a. In fact, the amplitude of decadal SLA in the EEIO is weak compared to SWIO and WAC

(Fig. 1a). The asociated negative SLA off the WAC potentially indicates the role of ENSO influencing these two regions (SWIO and WAC) via atmospheric and oceanic teleconnections, consistent with the previous studies.

SLA in the SWIO declined during the final decades of the twentieth century, roughly 1960 – 2000, and has since rebounded (Fig. 1c). This multi-decadal decline in sea level and heat content in the SWIO has been examined in previous research (e.g., Han et al., 2010; Jin et al., 2018). Decadal SLA in the SWIO exhibits a high during the 1960s, around 1980, towards the end of the 1990s, around 2005, and since 2015 (Fig. 1c). Decadal SLA also declined notably in the 1970s, 1980s, around 2000, and 2010. A regression of decadal WSC and SLP onto the SWIO sea level shows the SEIO as a key region of SLP/wind forcing (Fig. 1b). The SWIO sea level is correlated to the SEIO WSC (white rectangle in Fig. 1b) by 0.88, suggesting wind-driven Rossby wave dynamics, driving the decadal sea-level variations in the SWIO. There is an SLP high (black rectangle in Fig. 1b) in the SEIO associated with SWIO SLA that potentially drives the SEIO anti-cyclonic WSC (Fig. 1b). The SEIO WSC is correlated to SEIO SLP by 0.56 (Fig. 1c).

In the following sections, we describe the relative roles of climate modes in shaping the WSC (SLP) in the SEIO, which drive the SWIO SLA. We show that SST changes in the central equatorial Pacific (CEP) exert strong control on the SEIO SLP via atmospheric teleconnections, which, combined with intrinsic SLP changes in the IO, collectively explain decadal WSC and sea-level variations in the SWIO.

3.2. The role of Pacific forcing

A regression analysis of decadal SST, winds, and SLP onto the SWIO sea level (normalized by standard deviation) shows the central equatorial Pacific (CEP) as a potential region driving the SEIO SLP (WSC) through atmospheric teleconnection (Fig. 2). The maximum SST change occurs around the dateline, and the associated SLP pattern (a pan-Pacific pattern with negative anomalies centered over the Hawaiian Islands) resembles the central Pacific El Niño (ENSO-Modoki) reported in previous studies (e.g., Ashok & Yamagata 2009; Ashok et al., 2007; Lorenzo et al., 2010). As the EOFs of decadal SST in the tropical Pacific suggest (Fig. S3), the CEP SST warming can be associated with either decadal ENSO or ENSO-Modoki. Considering conventional definitions of climate indices for these Pacific modes hence brings covariance between the indices (Table S1). We hence used the first two PCs of the tropical Pacific decadal SST as indices for ENSO (EEI) and ENSO-Modoki (EMI) in this study, as shown in Fig. S3cd. A warming SST anomaly in the CEP (El Niño or positive Modoki) induces subsidence and an anti-cyclonic WSC in the SEIO (Fig. 2).

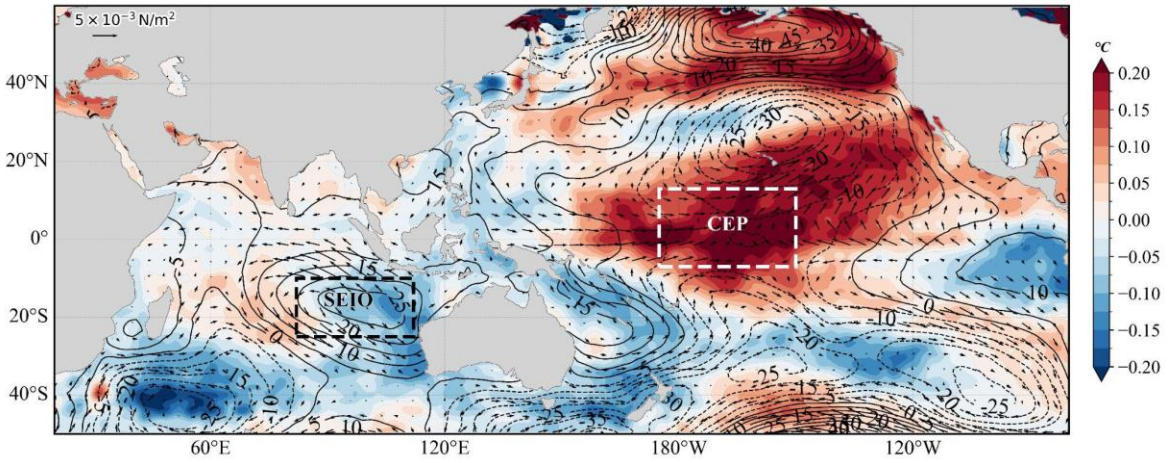


***Figure 2**: Regression of decadal sea surface temperature (SST; shading), SLP (contours; unit is mb), and wind stress (vectors) onto (normalised) decadal SLA averaged in the SWIO. The two regions with the highest regression coefficients for SST in the Central Equatorial Pacific (CEP) and for SLP in the Southeast Indian Ocean (SEIO) are highlighted by rectangles.*

The amplitude of Pacific warming is greater for Canonical ENSO; however, the corresponding SLP pattern in the IO is distinct for ENSO and ENSO-Modoki, as shown in Fig. 3a and Fig. 3b, respectively. Fig. 3a shows the typical SST and SLP response of the IO to an El Niño, as reported in several past studies, with basin-wide SST warming and positive SLP anomalies, indicating subsidence (Klein et al., 1999; Wu et al., 2021; He et al., 2020). On the other hand, the positive phase of the ENSO-Modoki (a warming of the CEP) exhibits weak negative SST anomalies in the IO with negative SLP anomalies elsewhere, except in the SEIO (Fig. 3b). A positive SLP maximum appears in the SEIO for both ENSO and ENSO-Modoki, with the strength of the SLP anomalies significantly higher for canonical ENSO than ENSO Modoki (Fig. 3a, b). However, WSC in the SEIO triggered by ENSO-Modoki is stronger than that induced by ENSO (Fig. S4a, b) and aligned geographically more with the SWIO sea-level related WSC (Fig. 1b). Together, the relative position and strength result in a stronger correlation ($r = 0.48$) between Modoki-related WSC and the original WSC in the SEIO than for ENSO ($r = 0.43$). Notably, the multi-decadal change of SEIO WSC (Fig. S4c) is linked to ENSO-Modoki. A 21-year moving trend of WSC in the SEIO suggests an in-phase multi-decadal relationship with ENSO-Modoki and an opposing change in WSC related to canonical ENSO (Fig. 3c). Despite the prominence of ENSO-Modoki in driving the SEIO WSC, the two flavors of ENSO have distinct teleconnection patterns in the IO, and both contribute to characterizing the WSC in the SEIO (Fig. 3a, b). A combined regression model of SEIO WSC, with EEI and EMI as predictors (methods), yields a correlation of 0.64 with the SEIO WSC, as shown in Fig. S4d.

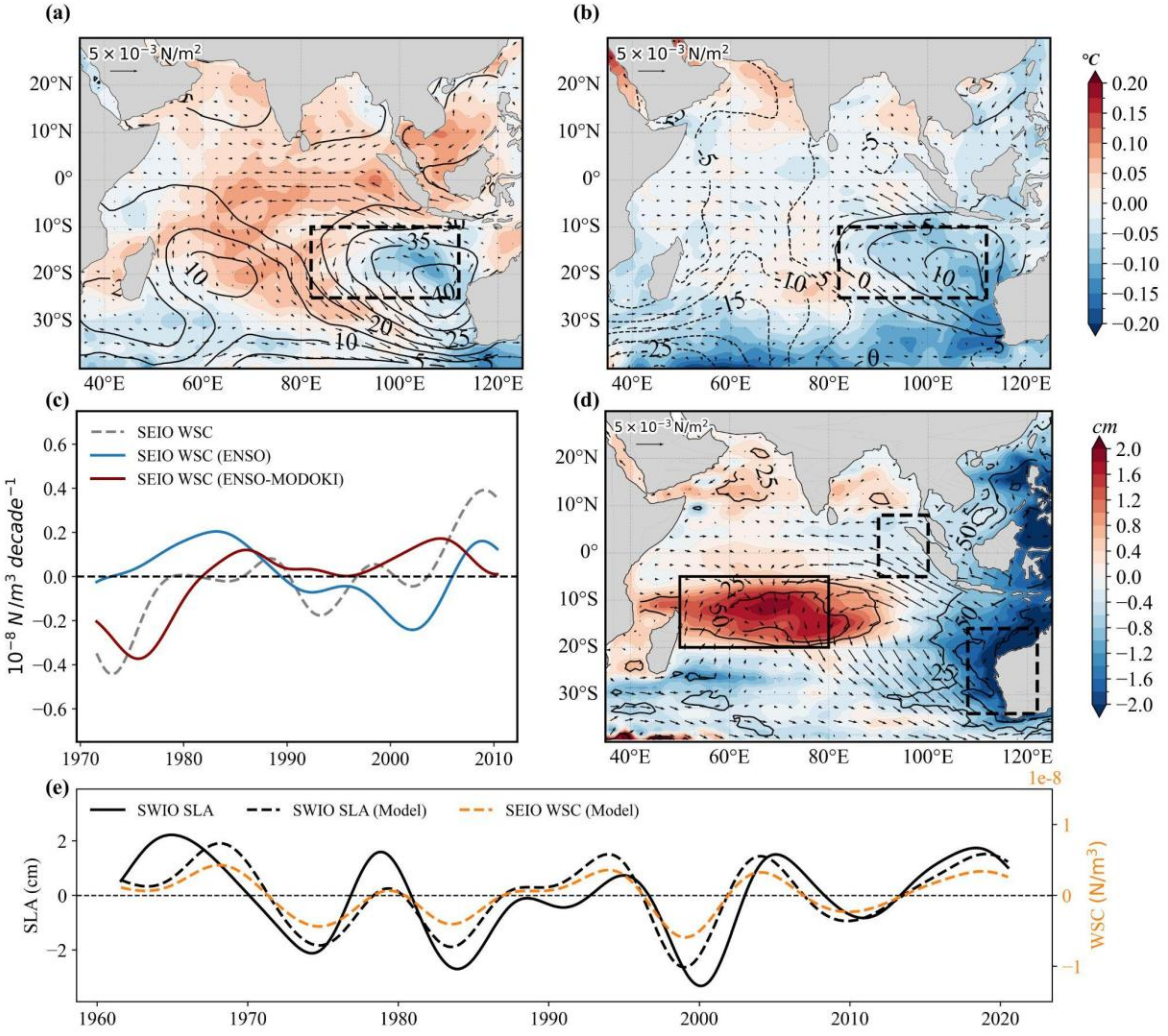


***Figure 3**: Regression of decadal SST (shading), SLP (contours; unit is mb), and wind stress (vectors) onto (normalised) (a) EEI (ENSO) and (b) EMI (ENSO Modoki) indices, respectively (methods). The region of the SLP maximum in the SEIO, corresponding to the SWIO SLA, is overlaid in panels a and b. (c) 21-year running trend of SEIO WSC (white rectangle in Fig. 1b) along with similar trend curves computed for a linear regression WSC model for the same region based on EEI (blue) and EMI (red). (d) Regression of decadal SLA (shading) and wind stress (vectors) onto the combined climate index based on EEI and EMI (methods). The contours show the explained variance of decadal SLA of the regression model with the combined index (see text). (e) Time series of SWIO SLA and SLA (WSC) estimated by a linear regression model based on EEI and EMI in the SWIO (SEIO).*

The influence of Pacific climate variability on SWIO sea level shall also operate through the oceanic bridge (see Schwarzkopf & Böning, 2011). Fig. S5, for instance, shows the lead-lag regression of sea level and wind onto the normalized sea level averaged in the SWIO region. The sea-level pattern at a lag of 4 years (i.e., four years before the SWIO sea-level maximum) indicates a negative phase of the decadal ENSO-related sea-level pattern in the Pacific (Fig. S5), with positive sea-level anomalies in the western Pacific and the SEIO. Those positive SLAs in the SEIO, however, seem to decay rapidly (weak SLA in lag -3 years), and the development of anticyclonic WSC in subsequent years tends to produce positive SLAs that propagate westward as Rossby waves, reaching the SWIO in about 1-2 years. A longitude-time plot of decadal SLA averaged between 5°S-20°S (the same latitudinal range of the SWIO sea-level box) reveals two things: First, the sea-level variability in the SEIO has become prominent

in the recent decades (post 1990s; Fig. 4a), and the variability is partly related to ENSO through the oceanic bridge (Fig. 4b). Secondly, those sea-level anomalies in the SEIO decay fast westward and last around 90E (Fig. 4a). The decadal SLA seen west of 90°E hence can be attributed largely to wind-driven. For instance, the SWIO decadal sea-level fall in the 1970s (Fig. 1c, Fig. 4a) is caused by ENSO-driven negative WSC (Fig. S4c and Fig. 4b), and a similar sea-level fall during the 1980s and towards the end of the twentieth century is related to ENSO-modoki driven negative WSC (Fig. 4a, c and Fig. S4c). Evidently, the multi-decadal variability in the SWIO SLA is mostly related to Modoki-driven WSC changes, and there are no oceanic bridge signals in the SEIO associated with decadal Modoki (Fig. 4c). Fig. 4 hence suggests that the Pacific influence on SWIO decadal SLA is largely wind-driven and occurring through atmospheric teleconnections driven by both ENSO and ENSO-Modoki. A combined regression model of decadal SLA with ENSO and Modoki indices (EEI and EMI) suggests that up to 50% of the SWIO sea-level variance is explained by the Pacific forcing (Fig. S6 and Fig. 3d). The regression model SLA for the SWIO correlate the SWIO averaged SLA by 0.81 (Fig. 3e). Notably, the decadal SLA response to Pacific forcing in the north IO (north of 10°S) is relatively weak (Fig. 3d), suggesting an influence confined to the southern tropical IO, consistent with previous studies (e.g., Nidheesh et al. 2013).

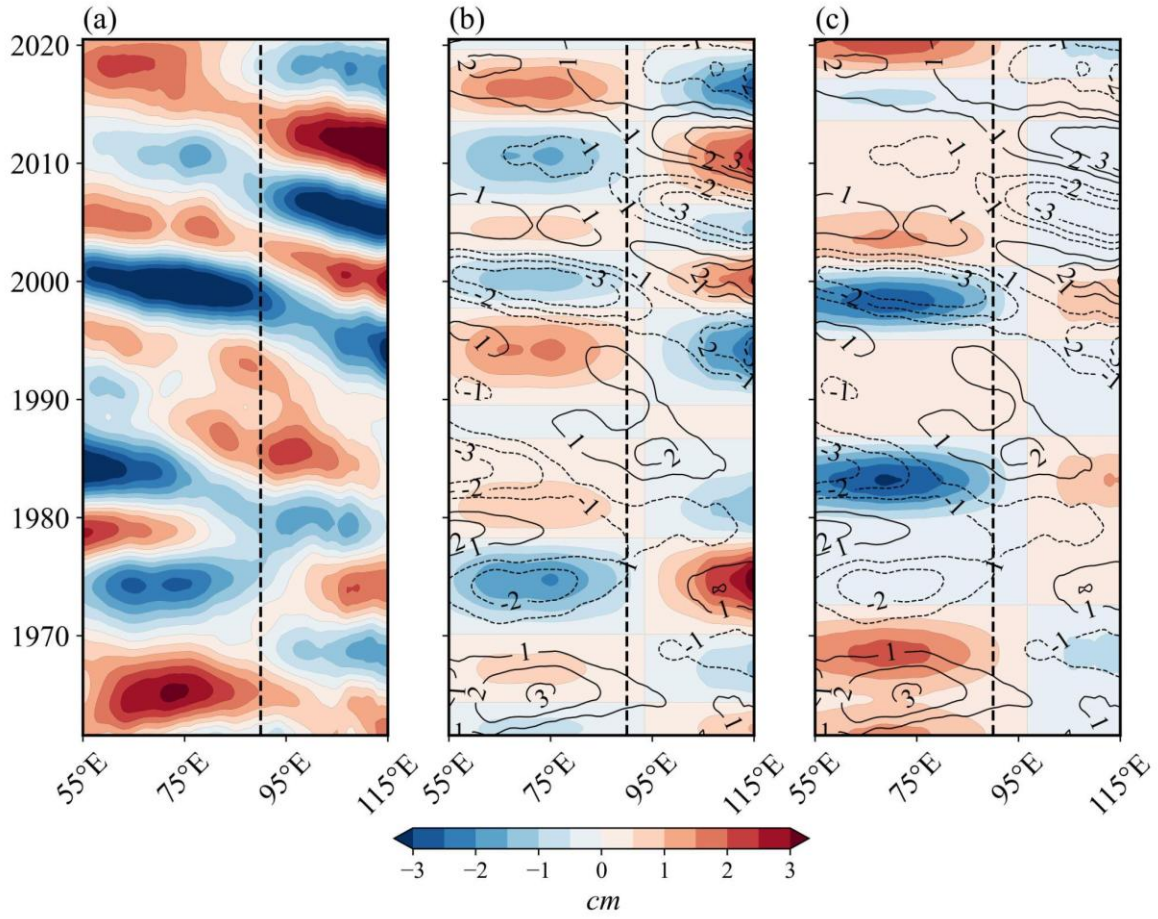


Figure 4*: Hovmöller diagram of (a) decadal SLA averaged between 5°S and 20°S (same latitudinal distance of the SWIO box defined in Fig. 1). b), c) are similar diagrams to a) but for the regressed decadal SLA onto EEI (ENSO) and EMI (ENSO Modoki), respectively. The SLA in panel (a) is overlaid in panels b) and c) as contours. A vertical line is drawn at 90°E to highlight the wind-driven SLA and SLA radiating from the eastern boundary on either side.*

3.3. Role of Local Wind Forcing

To isolate variability independent of Pacific forcing, we removed the effects of Pacific climate modes (represented by EEI and EMI) using a linear regression (methods) for sea level and other variables. In the following, we use the term "residual" to refer to this Pacific-independent Indian Ocean variability. Figure 5a shows the pattern of residual SLA and (residual) wind in the Indian Ocean associated with a one standard deviation change of residual SLA averaged in the SWIO (black box in Fig. 1a and Fig. 5a). The amplitude of SWIO residual SLA is reduced and shifted northwest (centered around 12^{o}S), and there are associated negative SLA in the EEIO and along the rim of the eastern Bay of Bengal, with weak signals in the SEIO (Fig. 5a). The associated wind-stress vectors indicate a WSC to the east of SLA maximum in the SWIO (Fig. 5a). The role of local WSC driving the decadal SLA in the SWIO is reported in the past (e.g. Zhuang et al. 2013; Nidheesh et al., 2013). We performed an EOF analysis of residual WSC over the region shown by the white dashed rectangle in Fig. 5a (we use the same WSC box definition for all figures in this paper). The EOF1 of residual WSC in the SIO shows a clear positive pattern, driving the SLA through Ekman pumping and Rossby wave dynamics (Fig. 5b). The PC1 of residual WSC is correlated to the SWIO residual SLA by 0.8 (Fig. 5e), indicating a strong in-phase relationship.

We examined whether known climate modes over the IO, other than the ENSO modes we already removed, influence this coupled variability of WSC and SLA using a linear correlation analysis of WSC PC1 with those climate indices (Table S2). We found no significant correlation between those climate indices and WSC, suggesting an "intrinsic" nature of residual WSC and SLA in the IO. In order to characterise the SLP pattern associated with the WSC, we regressed the residual SLP onto WSC PC1, and the regression pattern is shown in Fig. 5c. The SLP pattern exhibits a distinct high between 10-20S, with negative SLP anomalies to the south where the climatological Mascarene High is located (Fig. 5c). As the WSC is driven by the SLP gradient, following trials and previous studies (e.g., Thompson et al. 2016; Nidheesh et al., 2022), we found that the pressure centers north and south (shown by rectangles A and C in Fig. 5c) of the SLP high (region B) are pivotal in determining the intrinsic WSC in the SIO. Hence, we derived an SLP-based index considering those three pressure centers in the IO, termed the 'Indian Ocean Decadal Index (IDI)', representing the decadal SLP gradient across these three pressure centers as:

$$IDI = SLP_B - 0.5 \times (SLP_A + SLP_C);$$

where SLP_B, SLP_A, and SLP_C represent the residual SLP anomalies averaged at regions B, A, and C, respectively, as shown in Fig. 5c. The IDI is correlated to the WSC PC1 by 0.91 and to SWIO SLA by 0.80 (Fig. 5e).

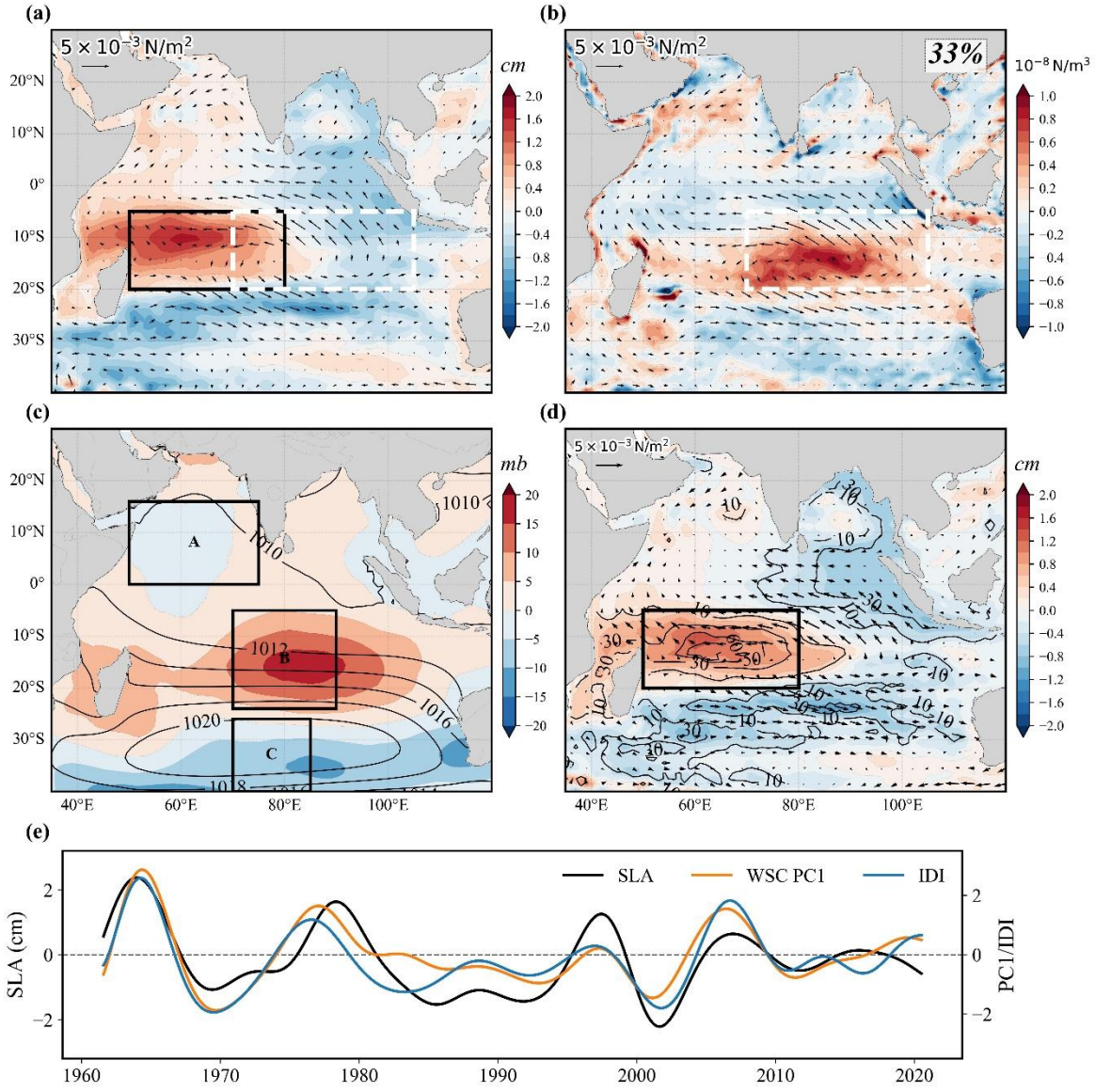


Figure 5: *(a) Regression of residual SLA (shade) and wind stress (vector) onto the (normalised) residual SLA averaged in the SWIO (black box). The key region of WSC in the SEIO is also shown by a white rectangle (same region as shown in Fig. 1b). (b) The spatial pattern of residual WSC (shade) and wind stress (vector) associated with the residual WSC EOF1 in the SEIO (white rectangle). The variance explained by WSC EOF1 is shown in the top-right. The corresponding normalised PC1 is shown in panel e. The spatial pattern of WSC and wind vectors is obtained by regressing these variables onto PC1. (c) Regression of residual SLP onto (normalised) WSC PC1 (shading) and climatological SLP (contours; unit is in mb). The rectangles represent the key regions where the residual SLP exhibits a basin-wide tripole pattern. These rectangles are used to average residual SLP for the calculation of the Indian Ocean Decadal Index (IDI;). (d) Regression of residual SLA onto the (normalised) IDI (shade) and the contours represent the residual SLA explained variance by IDI overlayed by regressed winds. (e) Time series of residual SLA averaged in the SWIO, residual WSC in the SEIO (white box in panel b), and normalised IDI.*

Fig. 5d shows the regressed pattern of residual SLA and wind onto the IDI (IDI-related WSC is shown in Fig. S7) which resembles the residual SWIO SLA pattern shown in Fig. 5a. The IDI explains upto 60% of residual decadal SLA in the SWIO (Fig. 5d). Note that the IDI also captures those negative SLA in the EEIO and along the rim of the eastern Bay of Bengal, and the corresponding equatorial wind anomalies (Fig. S7), indicating its effectiveness in representing the intrinsic SLA dynamics in the tropical Indian Ocean. A longitude-time plot of residual SLA averaged between 5°S-20°S suggests that the IDI indeed captures the wind-driven SLA west of 90°E where WSC effect is dominant, leaving residual SLA east of 90°E out during the entire period (Fig. 6). Interestingly, the SLA in the SEIO seems to experience more decadal variability in the recent decades, which is independent from Pacific and intrinsic IO forcing (Fig. 6b). Neverthless, those eastern boundary SLA seems to decays fast and do not contribute to the SWIO SLA which is the focus of this study (Fig. 6a).

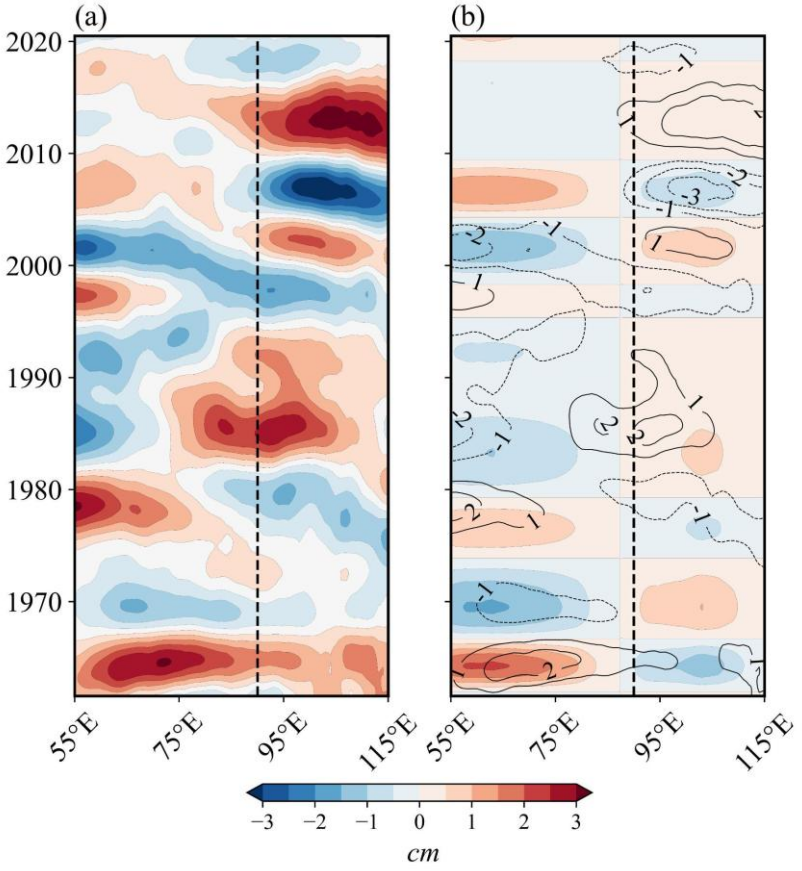


Figure 6: Hovmöller diagram of the (a) residual decadal SLA averaged between 5°S and 20°S (same latitudinal distance of the SWIO box defined in Fig. 1). b) Same as a) but for the regressed decadal SLA onto IDI. The SLA in panel (a) is overlaid in panel b) as contours. A vertical line is drawn at 90°E to highlight the wind-driven SLA and SLA radiating from the eastern boundary on either side.

3.4. Combined Model of SWIO SLA

We see that both the Pacific and the IO intrinsic climate variability shape the SWIO decadal SLA through wind-driven dynamics. A combined model of SWIO sea level (i.e., SLA regression pattern obtained combinedly from EEI, EMI and IDI; methods), which reflects both the Pacific forcing and intrinsic IO variability, agrees well with the observed SWIO decadal sea-level variability (Fig. 7a). The broad sea-level pattern in the IO with the maximum positive anomalies in the SWIO and negative anomalies off the WAC, EEIO, and eastern Bay of Bengal are well captured in the regression model (Fig. 7a), consistent to observation (Fig. 1a). The regression model also captures the related WSC and SLP patterns, as shown in Fig. 7b. The combined regression model explains up to 80% of the SWIO decadal SLA (Fig. 7a), and the regression model for the SWIO SLA (SEIO WSC) has a linear correlation coefficient of 0.94 (0.95) with observed SLA (WSC), as shown in Fig. 7c.

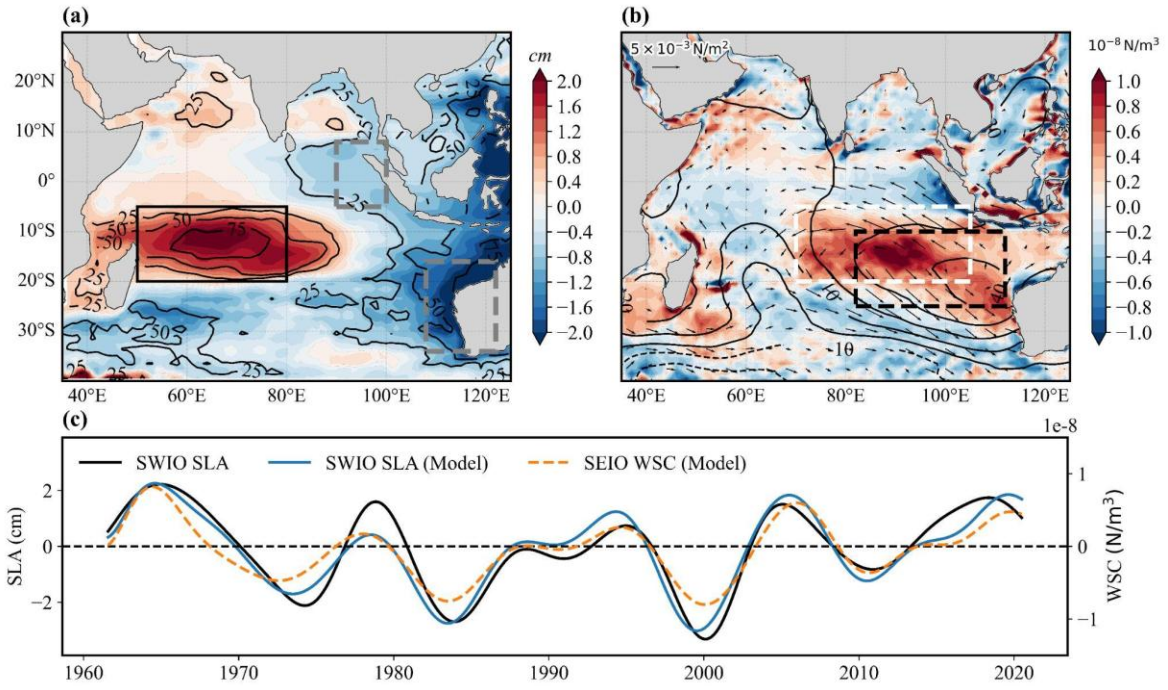


***Figure 7**: Regression of decadal SLA (shading) onto the (normalised) combined climate index comprising EEI, EMI, and IDI indices (methods). The contour represents the SLA-explained variance from the linear regression model based on this combined climate index. (b) Regression of WSC (shading), SLP (contours; units in mb), and wind stress (vectors) onto the combined index based on EEI, EMI, and IDI (methods). Time series of SWIO SLA and SLA (WSC) estimated by a linear regression model based on the combined climate index (comprising EEI, EMI, and IDI) in the SWIO (SEIO).*

4. Discussion

Sea-level variability in the SWIO is a key indicator of anomalous atmospheric circulation in the Indo-Pacific region. Fig. 2, for instance, represents the anomalous Walker circulation in the region where the climatological low-pressure centre is shifted from the Indo-Pacific warm pool to the central equatorial Pacific (CEP). Though the SLP and wind pattern in the Pacific in Fig. 2 is reminiscent of ENSO Modoki (e.g., Ashok et al. 2007; Behra

& Yamagata, 2010; Di Lorenzo et al., 2010), we show that both the Canonical ENSO and ENSO Modoki influence the IO circulation and sea level with distinct teleconnection signatures. A sea surface warming (cooling) in the CEP related to either ENSO or ENSO Modoki drives an anomalous subsidence (ascent) with an anti-cyclonic (cyclonic) wind-stress curl in the SEIO. However, our analyses show that, owing to the relative position and strength, ENSO Modoki exerts a stronger influence on decadal sea-level variability in the SWIO than canonical ENSO. Our results extend a similar finding of Behra and Yamagata (2010), who suggested a prominent decadal sea-level change in the SWIO in response to central Pacific warming in altimeter sea level (1993 – 2010).

One of the prominent features of sea level in the SWIO was a multi-decadal fall during 1960 – 2000, followed by its subsequent reversal (e.g., Alory et al., 2007; Han et al., 2010; Schwarzkoph & Boning, 2011; Nidheesh et al., 2013). Han et al. (2010) showed anomalous Walker and Hadley circulations in the Indian Ocean, partly modulated by anthropogenic warming of the Indo-Pacific warm pool, which drives this long-term ocean response. We show that long-term changes in SWIO sea level are linked to the multi-decadal variability of ENSO-Modoki and atmospheric teleconnections, rather than to the influence of the ENSO-driven oceanic bridge, as suggested by a few past studies (e.g., Schwarzkopf & Böning, 2011). This result indicates that, even though the Pacific trades weaken under global warming (a potential cause of negative SLA in the SEIO and SWIO via oceanic bridge and Rossby wave propagation), a central Pacific warming (pronounced Modoki) can induce positive SLA in the SWIO via atmospheric teleconnections. This mechanism explains the reversal of long-term sea-level fall in the SWIO around 2000, indicating a prominent role of central Pacific warming (ENSO Modoki) and atmospheric teleconnections over the Canonical ENSO (Schwarzkopf & Böning, 2011; Ummenhofer et al., 2017; Deepa et al., 2019) in shaping the SWIO long-term sea-level change.

We introduced a new decadal climate index, termed the Indian Ocean Decadal Index (IDI), to describe the SWIO residual sea-level variability and its forcing mechanism. The index is derived and named categorically to convey its role in basin-scale sea-level response – the IDI represents not only the residual WSC in the SIO but also the equatorial wind anomalies in the IO. The thermocline anomalies in the SWIO are responsive not only to the large-scale WSC but also to the local divergence between the southeasterly trades and the equatorial zonal wind anomalies in the IO (Herms & Reason, 2008). The residual sea-level response in the SWIO exhibits a distinct spatial pattern with a zonally elongated sea-level anomaly located equatorward (~10^{o}S; Fig. 5), indicating the potential role of zonal wind divergence shaping SLA, in addition to the WSC, which is centered further south (~15^{o}S). Consequently, the IDI also explains the opposite sea-level anomalies in the EEIO and along the rim of the eastern Bay of Bengal owing to the decadal equatorial winds associated with it. A moderate correlation (0.42) between decadal Mascarene High Index (MHI, not significant at 90% level) with the residual WSC (Table S2) potentially indicates a modulating effect of MH variability on southeasterly trades in the SIO, as previously suggested (Thompson et al., 2017; Nidheesh et al., 2022). The IDI, on the other hand, is able to explain the WSC rather efficiently by representing the residual SLP gradient across the entire tropical IO as shown in Fig. 5 (the linear correlation coefficient between the residual WSC and IDI is 0.84). Given these “basin-scale” atmospheric circulation characterising the residual decadal SLA in the tropical IO and the ability of IDI capturing it reasonably, we presume that the IDI nomenclature is adequate in future studies.

Our analyses suggest an emergence of pronounced decadal SLA in the SEIO in the recent decades which is independent from Pacific and intrinsic IO forcing (Fig. 6). The origin of these SLA appears to be south of Java where relatively larger amplitude of decadal sea-level variability is observed (contours on Fig. 1a). Though the ENSO-related oceanic bridge signal and alongshore winds south of Java partly drive these observed SLA (Figs. 3 & 4), there appears pronounced residual signals, especially post 1990's (Fig. 6). As the phase of those residual SLA coincides with ENSO SLA (Fig. 4), one possibility is the influence of a locally-sustained along-shore wind response off Java and northwest coast of Australia associated with Ningaloo Nino, which is shown to be influenced by La Nina conditions in the western Pacific (Kataoka et al., 2013; Feng et al., 2013; 2014). On the other hand, decadal variability may also emerge or be modulated by external forcing and climate change, as recently reported by Ding et al. (2024) for decadal SST variability in the SEIO. Nevertheless, as those eastern boundary residual SLA seem to decay rapidly and do not contribute to the SWIO SLA (Fig. 6a), exploring the causes of those residual SLA is beyond the scope of this study.

5. Conclusion

We show that the decadal sea-level variability in the southwest tropical Indian Ocean (SWIO; 5ºS-20ºS) is almost entirely wind-driven. The two ENSO flavors of ENSO, canonical ENSO and ENSO-Modoki, drive WSC in the SEIO through atmospheric teleconnections and shape the SWIO SLA via Rossby wave dynamics. Our results also show that the ENSO-Modoki plays a more prominent role in driving atmospheric teleconnections to the SIO than the canonical ENSO, thereby driving multi-decadal WSC variability. The SLP variability in the SEIO plays a key role in channelling the teleconnections between the two basins, with distinct spatial and temporal features. The SLP change associated with ENSO-Modoki is more aligned to the SWIO latitudinal band than the SLP anomalies associated with ENSO (which are shifted further southeast) and drives a more pronounced WSC in the SEIO. Once the Pacific contribution is removed, the geographic position of the residual WSC is seen shifted further westward (west of 90ºE and centered between 10ºS-20ºS), and the SLA response in the SWIO is also shifted northwest (centered 60ºE and 12ºS), more towards the region of seasonal thermocline ridge (e.g. Hermes & Reason, 2008; Zhuang et al., 2013). It is also noted that the SLA response to Pacific atmospheric teleconnection is confined to the SWIO region, with a weak SLA response in the north IO, while equatorial wind anomalies and SLA in the EEIO and along the rim of the Bay of Bengal are associated with the Indian Ocean Decadal Index (IDI). The observed multi-decadal decline and rebound of SLA over the last 50 years in the SWIO are linked to a similar multi-decadal change in central Pacific SST associated with ENSO-Modoki. Even though decadal ENSO drives SLA along the WAC through coastal wave-guide (with no or weak contribution from Modoki), the radiative effects of those eastern boundary SLA seem to be confined to south of 20ºS, as reported earlier (e.g., Deepa et al. 2018). In essence, our analyses untangle the distinct spatial and temporal fingerprints of locally and remotely driven decadal SLA in the SWIO.

References

Alory, G., Wijffels, S., & Meyers, G. (2007). Observed temperature trends in the Indian Ocean over 1960-1999 and associated mechanisms. *Geophysical Research Letters*, *34*(2). https://doi.org/10.1029/2006GL028044

Aparna, S. G., McCreary, J. P., Shankar, D., & Vinayachandran, P. N. (2012). Signatures of Indian Ocean Dipole and El Niño-Southern Oscillation events in sea level variations in the Bay of Bengal. *Journal of Geophysical Research: Oceans*, *117*(10). https://doi.org/10.1029/2012JC008055

Ashok, K., & Yamagata, T. (2009). The El Niño with a difference. *Nature*, *461*(7263). https://doi.org/10.1038/461481a

Ashok, K., Behera, S. K., Rao, S. A., Weng, H., & Yamagata, T. (2007). El Niño Modoki and its possible teleconnection. *Journal of Geophysical Research: Oceans*, *112*(11). https://doi.org/10.1029/2006JC003798

Barnett, T. P., D. W. Pierce, K. AchutaRao, P. Gleckler, B. Santer, J. Gregory, and W. Washington (2005), Penetration of human-induced warming into the World's Oceans, Science, 309, 284 – 287, doi:10.1126/ science.1112418.

Behera, S., & Yamagata, T. (2010). Imprint of the El Nio Modoki on decadal sea level changes. *Geophysical Research Letters*, *37*(23). https://doi.org/10.1029/2010GL045936

Cai, W., Hendon, H. H., & Meyers, G. (2005). Indian Ocean dipolelike variability in the CSIRO mark 3 coupled climate model. *Journal of Climate*, *18*(10), 1449–1468. https://doi.org/10.1175/JCLI3332.1

Carton, J. A., Chepurin, G. A., & Chen, L. (2018). SODA3: A new ocean climate reanalysis. *Journal of Climate*, *31*(17). https://doi.org/10.1175/jcli-d-18-0149.1

Chowdary, J. S., Gnanaseelan, C., & Xie, S. P. (2009). Westward propagation of barrier layer formation in the 2006-07 Rossby wave event over the tropical southwest Indian Ocean. *Geophysical Research Letters*, *36*(4). https://doi.org/10.1029/2008GL036642

Clarke, A. J., & Xiang Liu. (1993). Observations and dynamics of semiannual and annual sea levels near the eastern equatorial Indian Ocean boundary. *Journal of Physical Oceanography*, *23*(2). https://doi.org/10.1175/1520-0485(1993)023<0386:OADOSA>2.0.CO;2

Clarke, Allan J. (1991). On the reflection and transmission of low-frequency energy at the irregular western Pacific Ocean boundary. *Journal of Geophysical Research*, *96*(S01), 3289. https://doi.org/10.1029/90jc00985

Deepa, J. S., Gnanaseelan, C., Kakatkar, R., Parekh, A., & Chowdary, J. S. (2018). The interannual sea level variability in the Indian ocean as simulated by an ocean general circulation model. *International Journal of Climatology*, *38*(3), 1132–1144. https://doi.org/10.1002/joc.5228

Deepa, J. S., Gnanaseelan, C., Mohapatra, S., Chowdary, J. S., Karmakar, A., Kakatkar, R., & Parekh, A. (2019). The Tropical Indian Ocean decadal sea level response to the Pacific Decadal Oscillation forcing. *Climate Dynamics*, *52*(7–8). https://doi.org/10.1007/s00382-018-4431-9

Ding, M. H., Wang, X., Bian, L. G., Jiang, Z. N., Lin, X., Ren, S. H., Su, J., Tian, B., Wang, S., Yu, Y. N., Zhang, D. Q., Zhang, L., Zhang, W. Q., Zhao, S. D., & Zhu, K. J. (2025). State of polar climate (2024). Advances in Climate Change Research, 16(5). https://doi.org/10.1016/j.accre.2025.06.001

Feng, M., Meyers, G., Pearce, A., & Wijffels, S. (2003). Annual and interannual variations of the Leeuwin Current at 32°S. *Journal of Geophysical Research: Oceans*, *108*(11). https://doi.org/10.1029/2002jc001763

Feng, M., McPhaden, M. J., Xie, S. P., & Hafner, J. (2013). La Niña forces unprecedented Leeuwin Current warming in 2011. *Scientific Reports*, *3*. https://doi.org/10.1038/srep01277

Han, W., Meehl, G. A., & Hu, A. (2006). Interpretation of tropical thermocline cooling in the Indian and Pacific oceans during recent decades. *Geophysical Research Letters*, *33*(23). https://doi.org/10.1029/2006GL027982

Han, W., Meehl, G. A., Rajagopalan, B., Fasullo, J. T., Hu, A., Lin, J., et al. (2010). Patterns of Indian Ocean sea-level change in a warming climate. *Nature Geoscience*, *3*(8), 546–550. https://doi.org/10.1038/ngeo901

Hermes, J. C., & Reason, C. J. C. (2009). The sensitivity of the seychelles-chagos thermocline ridge to large-scale wind anomalies. *ICES Journal of Marine Science*, *66*(7). https://doi.org/10.1093/icesjms/fsp074

Hersbach, H., Bell, B., Berrisford, P., Horányi, A., Sabater, J. M., Nicolas, J., et al. (2019). Global reanalysis: goodbye ERA-Interim, hello ERA5. *ECMWF Newsletter*, (159).

Holgate, S. J., Matthews, A., Woodworth, P. L., Rickards, L. J., Tamisiea, M. E., Bradshaw, E., et al. (2013). New data systems and products at the permanent service for mean sea level. *Journal of Coastal Research*, *29*(3). https://doi.org/10.2112/JCOASTRES-D-12-00175.1

Jayasankar, T., Murtugudde, R., & Eldho, T. I. (2019). The Indian Ocean Deep Meridional Overturning Circulation in Three Ocean Reanalysis Products. *Geophysical Research Letters*, *46*(21), 12146–12155. https://doi.org/10.1029/2019GL084244

Jin, X., Kwon, Y. O., Ummenhofer, C. C., Seo, H., Schwarzkopf, F. U., Biastoch, A., et al. (2018). Influences of pacific climate variability on decadal subsurface Ocean heat content variations in the Indian Ocean. *Journal of Climate*, *31*(10). https://doi.org/10.1175/JCLI-D-17-0654.1

Kataoka, T., Tozuka, T., Behera, S., & Yamagata, T. (2014). On the Ningaloo Niño/Niña. *Climate Dynamics*, *43*(5–6), 1463–1482. https://doi.org/10.1007/s00382-013-1961-z

Klein, S. A., Soden, B. J., & Lau, N. C. (1999). Remote sea surface temperature variations during ENSO: Evidence for a tropical atmospheric bridge. *Journal of Climate*, *12*(4). https://doi.org/10.1175/1520-0442(1999)012<0917:RSSTVD>2.0.CO;2

Lee, T., & McPhaden, M. J. (2008). Decadal phase change in large-scale sea level and winds in the Indo-Pacific region at the end of the 20th century. *Geophysical Research Letters*, *35*(1). https://doi.org/10.1029/2007GL032419

Leith, C. E., (1973). The standard error of time-averaged estimates of climatic means. J. Appl. Meteor., 12, 1066–1069.

Lengaigne, A. G. N. M. (2013). Decadal and long-term sea level variability in the tropical Indo-Pacific Ocean, 381–402. https://doi.org/10.1007/s00382-012-1463-4

Li, Y., & Han, W. (2015). Decadal sea level variations in the Indian Ocean investigated with HYCOM: Roles of climate modes, ocean internal variability, and stochastic wind forcing. *Journal of Climate*, *28*(23), 9143–9165. https://doi.org/10.1175/JCLI-D-15-0252.1

Di Lorenzo, E., Cobb, K. M., Furtado, J. C., Schneider, N., Anderson, B. T., Bracco, A., et al. (2010). Central Pacific El Niño and decadal climate change in the North Pacific Ocean. *Nature Geoscience*, *3*(11). https://doi.org/10.1038/ngeo984

Masumoto, Y., & Meyers, G. (1998). Forced Rossby waves in the southern tropical Indian Ocean. *Journal of Geophysical Research: Oceans*, *103*(C12), 27589–27602. https://doi.org/10.1029/98JC02546

McCreary, J. P., Kundu, P. K., & Molinari, R. L. (1993). A numerical investigation of dynamics, thermodynamics and mixed-layer processes in the Indian Ocean. *Progress in Oceanography*, *31*(3), 181–244. https://doi.org/10.1016/0079-6611(93)90002-U

Mcphaden, M. J. (n.d.). *Genesis and Evolution of the 1997-98 El Niño*. Retrieved from https://www.science.org
Meyers, G. (1996). Variation of Indonesian throughflow and the El Niño - Southern Oscillation. *Journal of Geophysical Research: Oceans*, *101*(C5), 12255–12263. https://doi.org/10.1029/95JC03729

Mukhopadhyay, S., Gnanaseelan, C., Chowdary, J.S. et al. Prolonged La Niña events and the associated heat distribution in the Tropical Indian Ocean. Clim Dyn 58, 2351–2369 (2022). https://doi.org/10.1007/s00382-021-06005-2

Nidheesh, A. G., Lengaigne, M., Vialard, J., Unnikrishnan, A. S., & Dayan, H. (2013). Decadal and long-term sea level variability in the tropical Indo-Pacific Ocean. *Climate Dynamics*, *41*(2), 381–402. https://doi.org/10.1007/s00382-012-1463-4

Nidheesh, A. G., Lengaigne, M., Vialard, J., Izumo, T., Unnikrishnan, A. S., & Cassou, C. (2017). Influence of ENSO on the Pacific decadal oscillation in CMIP models. *Climate Dynamics*, *49*(9–10). https://doi.org/10.1007/s00382-016-3514-8

Pierce, D. W., Barnett, T. P., AchutaRao, K. M., Gleckler, P. J., Gregory, J. M., & Washington, W. M. (2006). Anthropogenic warming of the oceans: Observations and model results. *Journal of Climate*, *19*(10). https://doi.org/10.1175/JCLI3723.1

Potemra, J. T. (2001). Contribution of equatorial Pacific winds to southern tropical Indian Ocean Rossby waves. *Journal of Geophysical Research: Oceans*, *106*(C2). https://doi.org/10.1029/1999jc000031

Praveen Kumar, B., Vialard, J., Lengaigne, M. *et al.* Processes of interannual mixed layer temperature variability in the thermocline ridge of the Indian Ocean. *Clim Dyn* **43**, 2377–2397 (2014). https://doi.org/10.1007/s00382-014-2059-y

Rao, S. A., & Behera, S. K. (2005). Subsurface influence on SST in the tropical Indian Ocean: Structure and interannual variability. *Dynamics of Atmospheres and Oceans*, *39*(1-2 SPEC. ISS.). https://doi.org/10.1016/j.dynatmoce.2004.10.014

Saji, N. H., Goswami, B. N., Vinayachandran, P. N., & Yamagata, T. (1999). A dipole mode in the tropical Indian ocean. *Nature*, *401*(6751). https://doi.org/10.1038/43854

Schott, F. A., Xie, S. P., & McCreary, J. P. (2009). Indian ocean circulation and climate variability. *Reviews of Geophysics*, *47*(1), 1–46. https://doi.org/10.1029/2007RG000245

Schwarzkopf, F. U., & Bning, C. W. (2011). Contribution of Pacific wind stress to multi-decadal variations in upper-ocean heat content and sea level in the tropical south Indian Ocean. *Geophysical Research Letters*, *38*(12), 1–6. https://doi.org/10.1029/2011GL047651

Thompson, P. R., Piecuch, C. G., Merrifield, M. A., McCreary, J. P., & Firing, E. (2016). Forcing of recent decadal variability in the Equatorial and North Indian Ocean. *Journal of Geophysical Research: Oceans*, *121*(9). https://doi.org/10.1002/2016JC012132

Tozuka, T., Yokoi, T., & Yamagata, T. (2010). A modeling study of interannual variations of the Seychelles Dome. *Journal of Geophysical Research: Oceans*, *115*(4), 1–14. https://doi.org/10.1029/2009JC005547

599 Trenary, L. L., & Han, W. (2008). Causes of decadal subsurface cooling in the tropical Indian Ocean during 1961-
600 2000. *Geophysical Research Letters*, *35*(17). https://doi.org/10.1029/2008GL034687
601
602 Trenary, L. L., & Han, W. (2012). Intraseasonal-to-interannual variability of south indian ocean sea level and
603 thermocline: Remote versus local forcing. *Journal of Physical Oceanography*, *42*(4), 602–627.
604 https://doi.org/10.1175/JPO-D-11-084.1
605
606 Ummenhofer, C. C., Biastoch, A., & Böning, C. W. (2017). Multidecadal indian ocean variability linked to the
607 pacific and implications for preconditioning indian ocean dipole events. *Journal of Climate*, *30*(5).
608 https://doi.org/10.1175/JCLI-D-16-0200.1
609
610 Vialard, J., Shenoi, S. S. C., McCreary, J. P., Shankar, D., Durand, F., Fernando, V., & Shetye, S. R. (2009).
611 Intraseasonal response of the northern Indian Ocean coastal waveguide to the Madden-Julian Oscillation.
612 *Geophysical Research Letters*, *36*(14), 1–5. https://doi.org/10.1029/2009GL038450
613
614 Webster PJ, Moore AM, Loschnigg JP and Leben RR (1999). Coupled oceanic atmospheric dynamics in the
615 Indian Ocean during 1997-98. Nature 401:356-360.
616
617 Wijffels, S., & Meyers, G. (2004). An intersection of oceanic waveguides: Variability in the Indonesian
618 throughflow region. *Journal of Physical Oceanography*, *34*(5), 1232–1253. https://doi.org/10.1175/1520-
619 0485(2004)034<1232:AIOOWV>2.0.CO;2
620
621 Wu, C., Yeh, P. J. F., Ju, J., Chen, Y. Y., Xu, K., Dai, H., et al. (2021). Assessing the spatiotemporal uncertainties
622 in future meteorological droughts from CMIP5 models, emission scenarios, and bias corrections. *Journal of*
623 *Climate*, *34*(5). https://doi.org/10.1175/JCLI-D-20-0411.1
624
625 Xie, S. P., Annamalai, H., Schott, F. A., & McCreary, J. P. (2002). Structure and mechanisms of South Indian
626 Ocean climate variability. *Journal of Climate*, *15*(8). https://doi.org/10.1175/1520-
627 0442(2002)015<0864:SAMOSI>2.0.CO;2
628
629 Xie, S. P., Hu, K., Hafner, J., Tokinaga, H., Du, Y., Huang, G., & Sampe, T. (2009). Indian Ocean capacitor effect
630 on Indo-Western pacific climate during the summer following El Niño. *Journal of Climate*, *22*(3).
631 https://doi.org/10.1175/2008JCLI2544.1
632
633 Yu, W., Xiang, B., Liu, L., & Liu, N. (2005). Understanding the origins of interannual thermocline variations in
634 the tropical Indian Ocean. *Geophysical Research Letters*, *32*(24), 1–4. https://doi.org/10.1029/2005GL024327
635
636 Zhuang, W., Feng, M., Du, Y., Schiller, A., & Wang, D. (2013). Low-frequency sea level variability in the
637 southern Indian Ocean and its impacts on the oceanic meridional transports. *Journal of Geophysical Research:*
638 *Oceans*, *118*(3), 1302–1315. https://doi.org/10.1002/jgrc.20129
639
640 Zuo, H., Balmaseda, M. A., Tietsche, S., Mogensen, K., & Mayer, M. (2019). The ECMWF operational ensemble
641 reanalysis-analysis system for ocean and sea ice: A description of the system and assessment. *Ocean Science*,
642 *15*(3). https://doi.org/10.5194/os-15-779-2019
643

Data Availability

The ORAS5 reanalysis data are available from the European Centre for Medium-Range Weather Forecasts (ECMWF) at https://cds.climate.copernicus.eu/datasets. The SODA data and the GECCO data are hosted at http://dsrs.atmos.umd.edu/DATA/ and https://www.cen.uni-hamburg.de/en/icdc/data/ocean/easy-init-ocean/gecco2.html, respectively. The ERA5 wind fields are available from the Copernicus Climate Change Service via https://doi.org/10.24381/cds.f17050d7. Gridded altimeter data were downloaded from the Copernicus Marine Service (https://resources.marine.copernicus.eu/). Tide gauge data were obtained from https://psmsl.org/. Sea level pressure data were sourced from the NCEP reanalysis provided by NOAA Physical Sciences Laboratory (https://psl.noaa.gov/data/gridded/data.ncep.reanalysis.html). The HadISST sea surface temperature dataset is provided by the Met Office and is available at https://www.metoffice.gov.uk/hadobs/hadisst/. The codes used for data processing and analysis are available in the authors' GitHub repository.

Acknowledgements

We acknowledge the support provided by Director, Indian National Centre for Ocean Information Services (INCOIS), Ministry of Earth Sciences (MoES), Govt. of India, to conduct this research. The first author is grateful to CSIR, India, for the PhD fellowship, and to Kerala University of Fisheries and Ocean Studies (KUFOS) for providing the necessary facilities. This is INCOIS publication number xxx.

Funding

SCK received a research fellowship supported by the Council of Scientific and Industrial Research (CSIR), India towards his PhD research. The research is funded through the Deep Ocean Mission programme of the Ministry of Earth Sciences, India.

Conflict of interest

The authors have no relevant financial or non-financial conflicts of interests to declare.

Author Contributions

SCK and AGN conceptualized and designed the study. SCK performed data acquisition, analysis, and figure preparation, and drafted the initial version of the manuscript. AC provided overall supervision. All authors contributed to scientific discussions and writing of the manuscript.

Supplementary Files

This is a list of supplementary files associated with this preprint. Click to download.

- Supplymentaryinformation.docx